Involvement of Src-family tyrosine kinases in regulation of intraocular pressure: Src-family tyrosine kinase inhibitors as potential therapeutic agents for glaucoma

Tomoko Kirihara

Nara Institute of Science and Technology

Graduate School of Biological Sciences

Laboratory of Functional Neuroscience

Prof. Sadao Shiosaka

Submitted on 2013/1/22

Lab name (Supervisor)	Laboratory of Functional Neuroscience (Prof. Sadao Shiosaka)		
Name	Kirihara, Tomoko	Date	2013/11/30
Title	Involvement of Src-family tyrosine kinases in regulation of intraocular pressure: Src-family tyrosine kinase inhibitors as potential therapeutic agents for glaucoma.		

Abstract

The main risk and prognostic factor of glaucoma is elevated intraocular pressure (IOP). IOP level is determined by the balance between aqueous humor production and outflow from the eye. Agents acting on the conventional outflow route, the main pathway for draining aqueous humor, are expected to show stronger ocular hypotensive efficacy than the others which do not have an effect on this route.

Src-family tyrosine kinases (SFKs), a non-receptor tyrosine kinase family, are involved in the regulation of cell cytoskeleton and adhesion. Changes of cell cytoskeleton and adhesion of the trabecular meshwork (TM), a part of tissues composing the conventional outflow route, has been reported to regulate conventional outflow. Indeed, Rho-associated coiled-coil forming kinase (Rock) inhibitors have been reported to possess the ocular hypotensive efficacy that is assumed to be exerted at least partly by increased conventional outflow as a result of morphological changes in TM cells. Therefore, changes in SFKs activity can also be expected to have some roles in IOP regulation. However, there is no report that displays the functions of SFKs in ocular tissues and its

ocular hypotensive efficacy.

The purpose of this study is to assess an effect of SFK inhibitors on IOP. To this end, I first evaluated an ocular hypotensive efficacy of SFK inhibitors in ocular normotensive rabbits. SFK inhibitors significantly lowered IOP by intracameral injection. Then, I explored whether the ocular hypotensive efficacy of SFK inhibitors depends on an increase in conventional outflow using TM cells. PP2, an SFK inhibitor showing the most potent efficacy on IOP in this study, dose-dependently increased permeability of TM cell layers. At this time, PP2 decreased adhesion of TM cells to the culture surfaces either uncoated with specific ECM proteins dose-dependently or coated with extracellular matrix proteins and the tyrosine phosphorylation of focal adhesion kinase and $p130^{cas}$. On the other hand, major changes in actin staining and morphology of TM cells were not able to be detected after PP2 treatment, although quantitative analysis showed that PP2 induced some morphological changes. The effect of PP2 on TM cells was compared with Y-27632, a Rock inhibitor. Y-27632 increased permeability of TM cell layers and changed morphology of TM cells as previously reported, but did not change cell adhesion to the culture surfaces. These results suggested that SFK inhibitors lowered IOP, at least partly, by acting on TM cells in a manner that was distinct from Rock inhibitors.

List of Abbreviations

Abbreviations or Specialist Term	Explanation
BAK	Benzalkonium chloride, a detergent.
BFR	Bounding Box Area Fill Ratio, the ratio of the object's area to the area of its bounding rectangle box. The bounding box is the rectangle of minimum area that includes the object.
BME	Basement membrane extraction
CHAR	Convex Hull Area Ratio, the ratio of convex hull area to the object's area. The convex hull is defined as the smallest convex set containing the points of the object like a rubber band placed around the object.
ECM	Extracellular matrix
FAK	Focal adhesion kinase, a cytoplasmic protein, which directly interacts with Src family tyrosine kinases at focal adhesion sites and play important role in the SFK-mediated integrin-dependent signaling pathway. Maximal activity of FAK occurs after tyrosine phosphorylation by Src family tyrosine kinases.
IOP	Intraocular pressure
$p130^{cas}$	$p130^{cas}$ protein, a cytoplasmic protein, which is phosphorylated by Src family tyrosine kinases in various cellular events, including migration, survival, transformation, and invasion.
P2A	$Perimeter^2/4\pi$ Area, the ratio of length of object's perimeter to its area.
POAG	Primary open angle glaucoma, a type of glaucoma. The anterior chamber angle is open, and IOP elevation cannot be attributed to any other systemic and ocular factors.

Rock	Rho-associated coiled coil-forming protein kinase
SFK	Src-family tyrosine kinase
TEER	Trans-epithelial electrical resistance
TM	Trabecular meshwork, a tissue composing the conventional outflow route.

Introduction

Glaucoma is a major ocular disorder that can result in blindness via an irreversible loss of visual function (Quigley et al., 1996; Weinreb, 2007; Quigley, 2011). The main risk and prognostic factor so far supported by clinical evidences is elevated intraocular pressure (IOP) (the AIGS Investigators, 2000; Coleman and Miglior, 2008). Therefore, lowering IOP sufficiently to delay or prevent glaucomatous visual field loss is the most promising approach in current glaucoma treatment (Collaborative Nomal-Tension Glaucoma Study Group, 1998; Goel et al., 2010; Quigley, 2011). However, given that approximately half of glaucoma patients are adjunctively treated with 2 or more medications for appropriate IOP control (Kass et al., 2010; Kaneko et al., 2012), and that current medications are not effective in all patients (Camras et al., 2003; Choplin et al., 2004), there remains a need for novel pharmacotherapies which can deliver stronger or longer-lasting IOP-lowering efficacy for glaucoma treatment.

Aqueous humor is produced at non-pigmented epithelium of ciliary body, and leaves the eye via the outflow pathways at the anterior chamber angle (Figure 1, red and blue lines). Difference in formation and drainage rates of aqueous humor primarily determines the level of intraocular pressure (IOP), however, a main factor for the IOP level determination is the resistance offered to the drainage of aqueous humor (Gabelt and Kaufman, 2003; Goel et al., 2010). The route for the drainage of aqueous humor in the eye consists of two pathways, that is, the conventional (Figure 1, red solid line) and uveoscleral (Figure 1, red dash line) outflow routes. An increase in the resistance through the conventional outflow route (i.e., a decrease in the outflow facility) is considered to contribute to IOP elevation seen in primary open angle glaucoma (POAG) and during aging (Weinreb and Khaw, 2004; Gabelt and Kaufman, 2005; Acott and Kelley, 2008; Johnstone, 2009). Build-up of extracellular materials or loss of cells at the trabecular meshwork (TM), a part of tissues composing the conventional outflow route, are possible causes of the decrease in the outflow facility (Gabelt and Kaufman, 2005; Fuchshofer and Tamm, 2009), but the precise mechanism remains unclear. Given these, an agent that can increase conventional outflow would be expected to possess a strong IOP-lowering efficacy and improve the impaired function of the conventional outflow pathway. Therefore, I tried to find out a new agent that exhibits an IOP-lowering efficacy by increasing conventional outflow.

There is some evidence that an increase in conventional outflow is caused by changes in actin organization and/or a decrease in extracellular matrix (ECM). Contribution of actin organization on conventional outflow is suggested by the

researches using chemical agents that disrupt cytoskeleton including Rho-associated coiled coil-forming protein kinase (Rock) inhibitors and actin depolymerizers such as latrunculins. These agents lower IOP (Honjo et al., 2001; Okka et al., 2004; Gabelt and Kaufman, 2005; Tokushige et al., 2007; Fukunaga et al., 2009; Williams et al., 2011). Their ocular hypotensive efficacy is considered at least partly to be caused by increased conventional outflow, because they increased outflow facility in living rabbits and monkeys (Honjo et al., 2001; Tokushige et al., 2007; Okka et al., 2004; Tian and Kaufman, 2005) and in enucleated animal eyes (Rao et al., 2001; Lu et al., 2008) and increased permeability of Schlemm's canal endothelial cell layer (Rao et al., 2001), another tissue composing the conventional outflow route (Figure 1). The increase in conventional outflow is believed to be exerted by changes in actin organization of the TM and/or Schlemm's canal cells (Honjo et al., 2001; Rao et al., 2001). The changes in actin organization result in alterations in cell morphology, contraction conditions, and adhesion to cells or ECM. On the other hand, contribution of ECM on the increase in conventional outflow is suggested by the researches on matrix metalloproteinases (MMPs), which regulate ECM turnover. Increases in MMP activity increased outflow facility in the conventional outflow route (Bradley et al., 1998; Crosson et al, 2005).

Src-family tyrosine kinases (SFKs), cytoplasmic non-receptor type tyrosine kinases composed of Src, Fyn, Yes, Lck, Hck, Blk, Fgr, Lyn and Yrk, are expressed in a wide variety of cells and play key roles in regulation of proliferation, cytoskeletal alteration, differentiation, survival, adhesion, and migration (Thomas and Brugge, 1997; Elliott et al., 2011). This functional variety reflects their ability to interact with diverse classes of cellular receptors and distinct cellular targets. Moreover, a change in SFK activity is implied to cause pleiotropic reactions in cells. Src-transformed cells showed a loss of actin stress fibers as a result of suppression of Rho activity (Fincham et al., 1999), but conversely, there are reports that imply similar efficacy between inhibition of SFK- and Rho/Rock-mediated signaling pathways. PP2, a potent inhibitor of several SFKs with single-digit nanomolar inhibitory activity (Hanke et al., 1996; Jones et al., 2002), inhibits the phosphorylation of myosin light chain (MLC) induced by ECM proteins such as fibronectin, laminin, and collagen type IV in cultured TM cells, as does a Rock inhibitor (Zhang et al., 2008). Such similarity has been also observed in other cell-types, example being the prevention of transforming growth factor (TGF) β1-induced RhoA activation by Src inhibition in mesangial cells (Peng et al., 2008), and the disappearance of phospho-MLC from the cell periphery induced by PP2 and a Rock inhibitor in colon carcinoma cells

(Avizienyte et al., 2004). Given the functions of SFKs, the efficacy of SFKs inhibitors, and the regulation of conventional outflow, changes in SFKs' activity are likely to play some roles in conventional outflow. However, it has not known how SFKs function in ocular tissues, or whether SFK inhibitors display IOP-lowering efficacy.

The purpose of this study was to assess the potential of SFK inhibitors as prospective new ocular hypotensive agents. To this end, I first evaluated their effect on IOP in ocular normotensive rabbits. Having found that they were effective, I explored their potential mechanism by evaluating effects of PP2, a selected representative of the SFK inhibitors evaluated in this study, on the permeability of TM cell layers, morphology, adhesion, and tyrosine phosphorylation of focal adhesion kinase (FAK) and $p130^{cas}$ in TM cells, and by comparing them with the corresponding effects of a Rock inhibitor.

Materials and Methods

Chemicals and Drug Preparation

PP2 (4-amino-5-(4-chlorophenyl)-7-(t-butyl)pyrazolo[3,4-d]pyrimidine, MW=301.78, Figure 2-a), PP1 (4-amino-5-(4-methylphenyl)-7-(t-butyl) pyrazolo[3,4-d]pyrimidine, MW=281.36, Figure 2-b), SFK inhibitors, and PP3 (4-amino-1-phenylpyrazolo[3,4-d]pyrimidine, MW= 211.22, figure 2-d), a negative control of PP2 that lacks kinase inhibitory activity against SFKs, were purchased from Tocris (Elliswille, MO). Y-27632 dihydrochloride (4-[(1R)-1-aminoethyl]-n-pyridin-4-ylcyclohexane-1-carboxamide dihydrochloride, MW= 320.26, Figure 2-e), a Rock inhibitor, and damnacanthal (3-hydroxy-1-methoxy-9,10-dioxoanthracene-2-carbaldehyde, MW=282.25, Figure 2-c) , an SFK inhibitor, were purchased from Sigma-Aldrich (St Louis, MO) and Merck Millipore (Darmstadt, Germany), respectively. For the IOP study, the drug was dissolved in dimethyl sulfoxide (DMSO; Wako, Osaka, Japan) and diluted in saline to 1 mM, with a final DMSO concentration of 0.5%. For *in vitro* studies, the drugs were dissolved in DMSO and then diluted using 'experiment medium' [low glucose Dulbecco's Modified Eagle's Medium (DMEM; nacalai tesque, Kyoto, Japan) supplemented with 3% fetal bovine serum (FBS; Hyclone, Logan, UT), 2 mM L-glutamine, 25 μg/mL gentamicin, and 2.5 μg/mL amphotericin B] to yield 0.1-100 μM drug solutions with the final DMSO

concentration being 0.2%. In all treatments, 'vehicle' means the solvent at the same concentration as that in the drug solution.

Mouse monoclonal antibodies to human vinculin, human FAK, and human $p130^{cas}$ were purchased from Sigma, Millipore, and BD Biosciences (San Jose, CA), respectively. Rabbit polyclonal antibodies to phospho-FAK(Tyr^{576}) and phospho-$p130^{cas}$(Try^{410}) were purchased from Life technologies (Carlsbad, CA) and Cell Signaling Technology (Danvers, MA), respectively. Goat alexa fluor 488 conjugated anti-mouse IgG was purchased from Life technologies, and donkey horseradish peroxidase (HRP)-conjugated anti-mouse IgG and anti-rabbit IgG were purchased from Jackson ImmunoResearch Laboratories (West Grove, PA).

Animals

Japanese white rabbits (Kitayama Labes, Nagano, Japan) weighing 3.0 to 4.0 kg were used. All experiments were conducted in accordance with the ARVO statement for the Use of Animals in Ophthalmic and Vision Research and the internal ethics code for animal study of Santen Pharmaceutical Co., Ltd. Animals were housed under a 12-h light-dark cycle (light phase: 7 am – 7 pm; dark phase: 7 pm – 7 am).

IOP Measurement, Anesthesia, and Drug Administration

A calibrated pneumotonometer (Model 30 Classic; Reichert Inc., Depaw, NY) was used to measure IOP. IOP measurement was performed on conscious animals under local anesthesia induced by topical administration of 0.4% oxybuprocaine hydrochloride solution (Benoxil ophthalmic solution 0.4%, Santen Pharmaceutical, Osaka, Japan).

IOP was measured before and at 2, 4, 6, and 8 h after drug administration. Intracameral injections were made using a microsyringe (Hamilton, Reno, NV) fitted with a 30-gauge needle, the volume administered being 20 μL. Drug concentration in the anterior chamber was estimated at 100 μM for the reason that the administered drug (20 μL) was diluted 10-fold by aqueous humor (200 μL). All drugs and vehicles were administered unilaterally, with the fellow eye remaining untreated. Administration was performed at around 11 am in all experiments. Drug-induced IOP changes were firstly compared with baseline in IOP, and then compared with the vehicle-treated group. Baseline was measured 2 days before the

treatment day at each scheduled time point on the drug treatment day without drug administration.

Cell Culture

Primary human TM cell was purchased from ScienCell Research Laboratories (Carlsbad, CA) and maintained in 'maintenance medium' (low glucose DMEM supplemented with 10% FBS, 2 mM L-glutamine, 25 μg/mL gentamicin, and 2.5 μg/mL amphotericin B) at 37 ℃, under 5% CO_2. The trypsin-ethylene diamine tetra-acetic acid (EDTA) method using 0.05% trypsin and 0.02% EDTA diluted by Ca^{2+}, Mg^{2+} free phosphate buffered saline (PBS) was used for passage. Cells that had undergone subculture passage less than 12 times from thawed cells were used for the present work.

Trans-epithelial Electric Resistance (TEER) Measurement

TEER measurement in TM cell layers was selected as an *in vitro* model to evaluate changes in cell morphology and/or cell adhesion which can suggest changes in outflow resistance of the TM, on the basis of previous reports (Li et al., 2004; Russ et al., 2010). Changes in permeability of cell layers were detected as changes in TEER. TM cells were seeded onto the membrane insert (0.4 μm pore; upper chamber) of a Transwell (Coster; Corning Life Sciences, Acton, MA) in maintenance medium except in wells for blank. The TEER of cell layers was measured using a voltohmmeter (EVOMX and ENDOHM; World Precision Instruments, Sarasota, FL), as described previously (Li et al., 2004; Burke et al., 2004). After the presence of stable TEER had been confirmed for several days, the medium was replaced for 1 h with experiment medium. Then, vehicle or drugs (PP2, 0.1-100 μM; PP3, 100 μM; Y-27632, 10 μM) in experiment medium were applied individually to both the upper and the lower chambers. Y-27632 was a positive control and a comparator of PP2. On the other hand, PP3 was a negative control in order to evaluate whether the efficacy of PP2 is caused by its kinase inhibitory activity. The basis of the drug concentration was: PP2, kinase inhibitory activity (IC_{50}) and *in vivo* IOP-lowering efficacy; PP3, equivalency to the highest concentration of PP2; Y-27632, the previous report regarding its efficacy on cell permeability (Rao et al., 2001) and almost equivalent IOP-lowering efficacy to PP2 at 100 μM in a preliminary internal IOP study using ocular normotensive rabbits (data not shown). TEER was measured before and at 1, 2, and 3 h after drug

application. An average of TEER in the wells without cells (a blank value) was subtracted from measured values of TEER in each well with cells: net TEER was used for analysis. Time-changes in TEER by drugs were evaluated by actual net values, and TEER changes at 3 h from the pretreatment value for each well were compared with the vehicle-treated group as 100%. The data shown represent the average of 3 independent experiments; each experiment was performed in triplicate.

Morphological change Analysis

1. Confocal microscopy of F-actin and vinculin

TM cells were seeded at a density of $6x10^3$ cells per well in a BD BioCoat Collagen I culture slide 8-well chamber (BD Biosciences) in maintenance medium. After 48 h, medium was replaced with the experiment medium, then vehicle or drugs (PP2, 0.1-100 μM; Y-27632, 10 μM) in experiment medium were applied. Cells were treated for 3 h, washed twice with PBS, and fixed in 4% paraformaldehyde solution for 10 minutes. After washing with Tris-buffered saline (TBS) containing 0.2% triton X-100 (TBS-T), cells were permeabilized by TBS-T and blocked in TBS-T containing 1% bovine serum albumin (BSA). Cells were stained with mouse anti-human vinculin antibody (1/400 diluted by TBS containing 1% BSA) for overnight at 4 °C. After washing with TBS-T, goat alexa fluor 488-conjugated anti-mouse IgG (1/1,000) was incubated for 1 h at room temperature. After washing with TBS-T, cells were treated with rhodamin-phalloidine (1/120, Life technologies) for 20 minutes at room temperature. After several washes with TBS-T, and sealed with Slowfade (Life Technologies). A confocal scanning laser microscope (Carl Zeiss, Oberkochen, Germany) with a 20x objective lens was used to photograph the cells.

2. Quantitative analysis of morphological change

Changes in morphology of TM cells were evaluated quantitatively using Cellomics ArrayScan (Thermo Scientific, Waltham, MA). TM cells were seeded at a density of $2x10^3$ cells per well in a 96-well multiplate in maintenance medium. After 24 h, medium was replaced with experiment medium before drug treatment, the cells were exposed for 3 h to vehicle or drugs (PP2, 0.1-100 μM; Y-27632, 10 μM) in experiment medium. After 2 h of drug treatment, the cell body was stained with 2 μM calcein-AM solution (Dojindo Laboratories, Kumamoto, Japan), and 1 h

later the cells were fixed by incubation for 1 h in formaldehyde, at a final concentration of approximately 3.4%). After wash with TBS, cells were stained with Hoechst33342 (Dojindo Laboratories). After several washes, ArrayScan captured cell images at 10 visual fields per well at predefined locations, and analyzed cell morphology using the morphology application. As Figure 3-a shows, cells were excluded from the analysis following the operating instructions if 1) cell body detected as one cell possessed two or more nuclei, and 2) the whole cell body was not contained within the visual field.

Indexes used to evaluate morphological changes in addition to cell area were as follows: Perimeter^2/4π Area (P2A, the ratio of length of object's perimeter to its area); Bounding Box Area Fill Ratio (BFR, the ratio of the object's area to the area of its bounding rectangle box. The bounding box is the rectangle of minimum area that includes the object); Convex Hull Area Ratio (CHAR, the ratio of convex hull area to the object's area. The convex hull is defined as the smallest convex set containing the points of the object like a rubber band placed around the object). In used morphological indexes, a value deviated less from 1 unit indicates acquiring less irregularity (sometimes acquiring round shape). In contrast, a value deviated more from 1 unit indicates acquiring irregular shape: a value higher than 1 unit in P2A and CHAR; a value lower than 1 unit in BFR. Image of relationship among cell morphology, irregularity, and evaluation indexes is shown in Figure 3-b.

Morphological change was first analyzed using actual values of each index to determine the direction of change, and then using changes relative to the vehicle-treated values to evaluate strength of each drug's effect. The data represent the average of 3 independent experiments, and data for each experiment consisted of 8 wells.

Cell Adhesion Analysis

TM cells in maintenance medium were seeded at a density of 2x10^3 cells per well, and grown for 24 h, in either a 96-well multiplate with a tissue culture-treated surface (non-coated) or a 96-well multiplate coated with one of the following ECM proteins: laminin I, collagen type I and IV, fibronectin, vitronectin, or basement membrane extraction (BME) purified from Engelbreth-Holm-Swarm tumors in which the major components are laminin, collagen type IV, entactin and heparin sulfate proteoglycan (Trevigen, Gaithersburg, MD). Medium was replaced with experiment medium before drug treatment. Next, experiment medium, vehicle

or drugs (PP2, 0.1-100 μM; PP3, 100 μM; Y-27632, 10 μM) for non-coated multiplate, or vehicle or PP2 at 100 μM for ECM protein-coated multiplate, in experiment medium was applied. Calcein staining began 1 h before the end of drug treatment. After 3 h of drug treatment, the cells were fixed in formaldehyde solution for 1 h. After several washes with TBS-T, absorbance at excitation 485 nm/emission 535 nm was measured to determine the number of cells.

Changes in the number of cells attached to the culture surfaces were expressed as ratios to the vehicle-treated group (as 100%). The data represent the average of 3 or 4 independent experiments. Experiments using non-coated plates were performed in octuplicate; those using ECM protein-coated plates were done in quadruplicate or sextuplicate.

Tyrosine Phosphorylation of FAK and p130^{cas}

TM cells were seeded in 10-mm dishes in maintenance medium, and grown until sub-confluent. Medium was replaced with experiment medium before drug treatment, then either vehicle or drugs (PP2, 100 μM; Y-27632, 10 μM) in experiment medium was applied. Three hours after drug treatment, protein was extracted using M-PER extract solution (Thermo Scientific) containing protease inhibitor cocktail (Roche Diagnostics, Basel, Switzerland) and phosphatase inhibitor (Roche Diagnostics). Protein concentration was determined using Pierce BCA protein assay kit (Thermo Scientific). Reduction treatment of protein was conducted using 2-mercaptoethanol diluted by Laemmli sample buffer. Equal amounts of protein were then loaded onto 7.5% SDS-PAGE gels and separated by electrophoresis. Proteins were transferred to PDVF membrane by semi-dry method. Protein-transferred PDVF membranes were blocked in SuperBlock T20, TBS (Thermo Scientific) for overnight at 4 °C, and then incubated for 2 h at room temperature with rabbit polyclonal primary antibodies to phosphor-FAK (1/1,000) or phospho-p130^{cas} (1/500). After washing with TBS containing 0.1% tween 80 (TBS-T), the membranes were next incubated for 1 h at room temperature with secondary antibody (donkey HRP-conjugated anti-rabbit IgG, 1/80,000). Immunoreactivity was detected using Immobilon Western Chemilum HRP Substrate (Millipore), and signals were transferred to X-ray films. Following this process, IgG complex to phosphorylated proteins was stripped using Restore PLUS Western Blot Stripping Buffer (Thermo Scientific). The stripped membranes were again blocked with SuperBlock for 1 h at room temperature, and reprobed with mouse monoclonal antibodies to FAK (1/1,000) or p130^{cas} (1/1,000) for 1 h at

room temperature. After washing with TBS-T, membranes were incubated with donkey HRP-conjugated anti-mouse IgG (1/40,000) as secondary antibody for 1 h at room temperature. After washing with TBS-T, immunoreactivity was again detected using Immobilon, and signals were transferred to X-ray films. Phosphorylation level relative to total protein was quantitatively evaluated using an image analyzer. The data represent the average of 2 independent experiments. Each sample was measured in duplicate.

Cell Viability

Changes in cell viability were evaluated using CytoTox-Glo Cytotoxicity Assay (Promega, Fitchburg, WI). CytoTox-Glo detects cell death by degradation of AAF-Glo substrate, a luminogenic peptide substrate, by activity of dead-cell proteases which are released from cells that have lost membrane integrity.

TM cells were seeded at a density of $2x10^3$ cells per well in a 96-well multiplate in maintenance medium, and grown for 24 h. Medium was replaced with experiment medium before drug treatment, then either vehicle or drugs [PP2, 0.1-100 μM; benzalkonium chloride (BAK, Wako), 10 ppm] in experiment medium was applied. BAK was a positive control of cell death inducer on TM cells (Ammar and Kahook, 2011). Three hours after drug treatment, AAF-Glo substrate solution was added and incubated for 15 minutes at room temperature after mixing. Luminescence, representing the number of dead cells, was measured using and ARVO SX Multilabel counter (Wallac, Turku, Finland). Subsequently, cell lysis regent including digitonin was then added and incubated for 15 minutes at room temperature after mixing. Luminescence, representing the number of total cells, was again measured.

Cell death was evaluated as the ratio of dead cells to total cells. The data represent the average of 3 independent experiments. Each experiment was performed in octuplicate.

Data Analysis

In the IOP study, data were analyzed by paired *t*-test for comparison with baseline, and by F-test for equality of variance and then Student's *t*-test for comparison with vehicle. In TEER evaluation, quantitative morphological change analysis, cell adhesion analysis using non-coated multiplates, and cell viability

analysis, data were analyzed by a sequence of Bartlett, one-way ANOVA, and Dunnett or Steel tests between the vehicle- and PP2-treated groups; for PP3, Y-27632, experiment medium, and BAK in these analysis and PP2 in adhesion analysis using ECM protein-coated multiplates, F-test followed by Student's *t*-test or Aspin-Welch's *t*-test were performed. $P < 0.05$ was considered to indicate statistical significance.

Results

Effects of SFK inhibitors on IOP

I evaluated the IOP-lowering efficacy of three SFKs inhibitors: PP2, PP1, and damnacanthal. Compounds at 1 mM were injected into unilateral eyes at around 11 am in ocular normotensive rabbits.

There were no significant differences in the IOP at time 0, between baseline and the treatment day in individual group, and across for groups at the treatment day. The IOP increased toward the dark phase in all groups at baseline and in the vehicle-treated group on the treatment day, reflecting the circadian change in IOP normally seen in ocular normotensive rabbits (Akaishi et al., 2005). All of the evaluated SFK inhibitors showed significant IOP-lowering efficacy compared with baseline, while vehicle did not cause IOP change (Figure 4-a and b). PP2 injection significantly lowered IOP in both actual IOP values and changes from time 0 at all measurement points except 2 h in changes from time 0, and tis maximal IOP reduction from baseline was about 8 mmHg at 8 h. Significant efficacies of PP1 and damnacanthal were observed at several measurement points: PP1, at 6 and 8 h in actual IOP values and at 2 and 4 h in changes from time 0; damnacanthal, at 4 and 6 h in changes from time 0. PP2 and damnacanthal also showed significant IOP-lowering efficacy in comparison with the vehicle-treated group (Figure 4-a and b). IOP values after PP1 injection were consistently lower, albeit not significantly so, than those for the vehicle-treated group (Figure 4-a and b). Both analyses (intra- and inter-group comparison) demonstrated that PP2 displayed the strongest efficacy among the evaluated SFK inhibitors, therefore PP2 was selected for further investigation of the mechanism by which SFK inhibitors show IOP-lowering efficacy.

Effect of PP2 on permeability in TM cell layers

Since SFKs play key roles in the regulation of cytoskeletal alteration (Thomas and Brugge, 1997; Elliott et al., 2011), I hypothesized that the IOP-lowering efficacy of SFK inhibitors is exerted by increasing outflow facility via the conventional outflow route, as is the case for Rock inhibitors and latrunculins which change actin organization enhance outflow via the conventional outflow route (Honjo et al., 2001; Rao et al., 2001; Okka et al., 2004; Gabelt and Kaufman, 2005; Tian and Kaufman, 2005; Lu et al., 2008).

To explore this hypothesis, the effect of PP on permeability of TM cell layers was evaluated using Y-27632 as a positive control. PP2 ranging from 0.1 to 100 μM dose-relatedly decreased TEER at all measurement points (Figure 5-a). TEER for 10 and 100 μM PP2 at 3 h after drug application decreased significantly to 79.5% and 71.7%, respectively, relative to the vehicle-treated group (Figure 5-b). Y-27632 at 10 μM induced a weaker but significant TEER decrease (to 83.4% of the vehicle-treated group) at 3 h after drug application compared to PP2 at the same concentration (Figure 5-b). On the other hand, PP3, a negative control compound lacking kinase inhibitory activity, had no effect on TEER throughout the evaluated period (Figure 5-a and b).

The decrease in TEER of TM cell layers by PP2 and Y-27632 suggested their IOP-lowering efficacies at least partly via the increase in conventional outflow.

Effect of PP2 on morphology of TM cells

An increase in conventional outflow is suggested to be caused by morphological and/or adhesion changes of cells or a decrease in ECM as described in the Introduction section. Given the key roles of SFKs on cytoskeletal alternation, I evaluated an effect of PP2 on cell morphology of TM cells to explore the potential mechanism of PP2-induced decrease in TEER. Morphological change at 3 h after the drug exposure was evaluated by actin and vinculin stain and measurement of four indexes in morphology application of ArrayScan: cell area, P2A, BFR, and CHAR.

Vehicle-treated TM cells showed elongated and flat shape with actin stress fibers (Figure 6-a). PP2 did not induce an obvious change in TM cell morphology, including changes in the distribution of actin and vinculin stain, even at 100 μM, the highest concentration (Figure 6-b, c, d, and e). On the other hand, Y-27632

changed the shape of TM cells like to spindle-like, with longer and thinner protrusions than those of the vehicle-treated cells, and caused the disappearance of actin stress fibers (Figure 6-f). On the other hand, the change of vinculin stain by Y-27632 was not clear (Figure 6-f).

Morphological change was quantitated using ArrayScan, an automated fluorescent imager. The average of analyzed cell number (mean ± SD) in each group ranged from 367.7 ± 88.5 to 774.0 ± 174.1 (Table 1). In an analysis using actual values, PP2 did not induce a significant morphological change for three of the four indexes, the exception being a decrease (i.e., the value deviated less from 1 unit) in CHAR at 10 μM (Table 2-a). In the analysis using ratios to the vehicle-treated group, in addition to the decrease in CHAR at 10 μM, an significant increase in BFR at 10 μM and decrease in CHAR at 100 μM PP2 were also detected, but there were no-dose-related changes (Table 2-b). Although morphological changes induced by PP2 were very slight, TM cells appeared to acquire less irregularity. On the other hand, Y-27632 at 10 μM induced significant changes on all indexes except cell area in both analyses (Table 2-a and b): P2A and CHAR increased and BFR decreased, compared to the vehicle-treated group (i.e., these values for the Y-27632-treated group all deviated more from 1 unit). These data demonstrate that Y-27632-treated TM cells acquired more irregularity. Therefore, the morphological change induced by PP2 was in the different direction from that of Y-27632, and changes relative to the vehicle-treated group were weaker than those induced by Y-27632, even though the efficacy of PP2 on TEER was dose-related and stronger than that of Y-27632 (Figure 5).

These results suggested that PP2 has a modest effect on TM cell morphology as shown in changes in CHAR and BFR, and that the direction of the effect on cell morphology by PP2 differs from that by Y-27632.

Effect of PP2 on adhesion of TM cells

Since PP2 did not induce obvious changes in TM cell morphology compared with Y-27632, I subsequently evaluated a TM cell adhesion change as a possible cause of PP2-induced decrease in TEER.

After confirming that the vehicle itself did not affect the adhesion of TM cells by comparison with the experiment medium-treated group (absorbance [mean ± SD]: medium, 1409.5 ± 308.9; vehicle, 1463.4 ± 200.7. There was no significant difference), the effects of drugs were evaluated by comparison with the

vehicle-treated group. The number of TM cells remaining attached to the non-coated surface after the PP2 treatment for 3 h decreased in a dose-dependent manner from 0.1 to 100 μM (Figure 7). The proportion of remaining cells for 0.1, 1, 10, and 100 μM PP2 was 99.2%, 95.4%, 86.1% and 74.0%, respectively, relative to the vehicle-treated group, and the changes at 1 μM and higher were significant. These reduction ratios were well consistent with those obtained in TEER experiment (Figure 5-b). On the other hand, neither PP3 at 100 μM nor Y-27632 at 10 μM decreased TM cell adhesion under the same conditions.

PP2 at 100 μM also significantly decreased the number to cells attached to surfaces coated with BME, laminin I, collagen type I, and fibronectin (Figure 8-a, b, c, and d) to 83.8%, 74.1%, 84.3%, and 81.6%, respectively, relative to the vehicle-treated group. Adhesion to surfaces coated with collagen type IV and vitronectin did not change significantly, although the mean values indicated comparably high degrees of reduction (Figure 8-e and f, reduction to 81.1% and 80.7%, respectively). Moreover, PP2-induced decrease in the number of cells attached to ECM-coated surfaces appeared to be consistent with that to the non-coated surface (reduction to 74.0%, Figure 7).

Effect of PP2 on tyrosine phosphorylation of FAK and p130^{cas}

On the regulation of adhesion dynamics by SFKs, there are both kinase-dependent and kinase-independent mechanisms (Jones et al., 2002). Since PP2 is a tyrosine kinase inhibitor (Hanke et al., 1996; Jones et al., 2002), PP2-induced changes in the TM cell adhesion is assumed to depend on a kinase-dependent mechanism. To clarify this hypothesis, I evaluated tyrosine phosphorylation of FAK and p130^{cas}, which are cytoplasmic proteins and directly interact with SFKs via the Src SH2 domain at focal adhesion. Through the phosphorylation at tyrosine residues of both FAK and p130^{cas} by SFKs, FAK and p130^{cas} play important role in the SFK-mediated integrin-dependent signaling pathway involving various cellular events such as migration, survival, transformation, and invasion (Thomas and Brugge, 1997; Playford and Schaller, 2004; Harburger and Calderwood, 2009).

Both PP2 at 100 μM and Y-27632 at 10 μM clearly decreased the tyrosine phosphorylation both of FAK at Tyr^{576} and of p130^{cas} at Tyr^{410} after drug exposure for 3 h (Figure 9-a and b, upper panels). Reprobing membranes verified that similar amounts of FAK and p130^{cas} were present in each lane (Figure 9-a and b, lower panels). PP2 decreased tyrosine phosphorylation of FAK and p130^{cas} by 93%

and 87%, respectively, relative to the vehicle-treated groups (Figure 9-c and d). PP2 at 100 μM displayed higher efficacy for both FAK and $p130^{cas}$ than Y-27632 at 10 μM.

Cell viability

Finally, I evaluated whether PP2 causes TM cell death, because cell death can reduce the attached cell number. A 3-h exposure of cells up to 100 μM PP2 did not increase the number of dead cells (Figure 10). Since the medium was not replaced after drug exposure in this study, all drug-treated cells including detached cells were evaluated. No increase in the number of dead cells by PP2 demonstrated that PP2 did not cause cell death and that the PP2-indeuced decrease in attached cells was not a result of cell death. In contrast, BAK, used as a positive control as it induced TM cell death (Ammar and Kahook, 2011), induced a significant increase compared with the vehicle-treated group (Figure. 10).

Discussion

I first showed that SFK inhibitors lowered IOP. Although all evaluated SFK inhibitors showed IOP-lowering efficacy, the efficacy profile among them was different. Enzyme inhibitory activity of PP1 was equivalent to that of PP2 (Hanke et al., 1996), however, the efficacy of PP1 was weaker than that of PP2 (Figure 4-a and b). Drug-induced changes in IOP may be affected by not only their enzyme inhibitory activity, but also penetration ability to cell membranes affected by chemical structure and/or physicochemical properties.

Concerning the relationship among the effects of Rock inhibitors and fibronectin on IOP, outflow facility, and permeability of the cell layer, changes in permeability of the TM and/or Schlemm’s canal cell layer are involved in the control of IOP and outflow facility through the conventional outflow route (Rao et al., 2001; Li et al., 2004; Fleenor et al., 2006). Therefore, the observed PP2-induced decrease in TEER of TM cell layers (i.e., increase in the permeability of the cell layer) suggested that the IOP-lowering efficacy of SFK inhibitors at least partly depends on the enhancement of conventional outflow. Moreover, the present studies clearly demonstrated that, at the cellular level, the primary mechanism of action of PP2 responsible for the decrease in TEER was to reduce

TM cell adhesion to culture surfaces coated with and without ECM proteins without significant loss of viability or direct toxicity (Figures 7, 8, and 10). The reported efficacy of the heparin II domain of fibronectin on outflow facility suggests that interference with cell-ECM interactions at the conventional outflow route results in an increase in outflow facility (Santas et al., 2003). The decrease in cell-ECM interactions may allow the conventional outflow route to expand the space available for aqueous humor drainage, i.e., to increase the porosity of this route. Therefore, the PP2-induced decrease in cell-ECM interactions is also likely to support the enhancement of conventional outflow by PP2. Additionally, this change suggests that PP2 has a potential to change outflow facility via the uveoscleral outflow route, which is another pathway for drainage of aqueous humor in the eye. Next research targets, therefore, are *in vivo* aqueous humor dynamics studies including uveoscleral outflow and aqueous humor formation, which were not focused in this study, to clarify mechanism of SFK inhibitors on IOP-lowering efficacy.

The PP2-induced decrease in TM cell adhesion to ECM proteins suggested that PP2 has a potential to change the signal transduction from integrins resulting in changes in focal adhesion because ECM proteins such as fibronectin, laminin, and collagen are recognized by integrins and ligation of these to integrins leads to transduction of intracellular signals (Playford and Schaller, 2004; Humphries et al., 2006; Harburger and Calderwood, 2009). PP2 reduced tyrosine phosphorylation of FAK and $p130^{cas}$ (Figure 9), which directly interact with SFKs and play important roles in the SFK-mediated integrin-dependent signaling pathway (Thomas and Brugge, 1997; Playford and Schaller, 2004). The lack of efficacy of PP3 on TEER and TM cell adhesion (Figures 5 and 7) also supports the notion that the efficacy of PP2 depends on its kinase inhibitory activity. The formation of focal adhesion complexes requires tyrosine phosphorylation of these proteins (Thomas and Brugge, 1997; Playford and Schaller, 2004; Harburger and Calderwood, 2009). Therefore, the PP2-induced decrease in TM cell adhesion may be a result of prevention of intercellular signaling via integrin and disassembly of focal adhesion complexes. In addition, the variety of PP2-induced decreases in TM cell adhesion according to the type of ECM protein suggests the specificity of molecular mechanism of PP2 on TM cell adhesion and/or the efficacy of PP2 in *in vivo* situation. One possible molecule relating the specificity is myocilin, a protein localized to both intracellular and extracellular sites in the TM. Ueda et al. reported that strong interactions under the biochemical conditions were observed between myocilin and fibronectin, laminin, and collagen type I, but moderate-to-weak and no interaction was displayed with vitronectin and collagen

type IV, respectively (Ueda et al., 2002). The difference in effects by PP2 on TM cell adhesion among ECM proteins, therefore, may be induced by the TM cell interactions to ECM in which myocilin takes part.

The PP2-induced morphological change toward less irregularity, suggesting a diminution of protrusions, may be related to uniform decreases in cell adhesion along with peripheral area. The lack of detectable changes in actin stress fibers in response to PP2 appears to be reasonable, because another SFK inhibitor, SU6656, did not affect RhoA activity without TGF-β stimulation in mesangial cells (Peng et al., 2008). However, morphological assays accompanied by several washes limited the evaluation targets to the remaining TM cells upon culture surfaces. As shown by adhesion assays, PP2 decreased the number of attached cells (Figures 7 and 8). Therefore, further studies that can evaluate changes in morphology and actin including detached cells are required to clarify the effect of PP2 on them.

Although the present study lacked an approach to detached cells by PP2, the results of the morphological assay and adhesion assay suggested that the effects of PP2 on TM cells differ from those of Y-27632 on the order of changes: PP2, adhesion change first and Y-27632, morphological change first. In addition, the profile of their IOP-lowering efficacy was different. The onset timing of IOP-lowering efficacy by Y-27632 was faster than that of PP2 (Honjo et al., 2001). Taken together, the primary molecular mechanism of PP2 in TM cells is likely to cause the difference in the profiles of their IOP-lowering efficacy.

In summary, SFK inhibitors displayed an ocular hypotensive efficacy, which may be caused by an increase in conventional outflow as a result of the decrease in TM cell adhesion. The mechanism of SFK inhibitors in IOP control is likely to differ from that of Rock inhibitors. Although further investigations are needed to clarify a specificity of SFK inhibitory activity on IOP-lowering efficacy, effects of SFK inhibitors on aqueous humor dynamics and ECM in *in vivo* situation, details of molecular and functional changes by SFK inhibitors relating to morphology and adhesion, and the difference between SFK inhibitors and Rock inhibitors, and TM cells used in these studies have a limitation for validating our finding because they were provided from one donor, SFK inhibitors, including PP2 or a related agent, show promise as new ocular hypotensive drugs.

Acknowledgements

I would like to express my sincere gratitude to my supervisors, Professor Shiosaka and Dr. Shimazaki for critical guidance and counseling of this research. I would like to express my appreciation to my supervisors, Dr. Ishikawa, Dr. Nakamura, and Dr. Tamura for their guidance that made my research of great achievement. I am very grateful to Ms. Yamashita for her valuable cooperation in my experiments. I am also very grateful to Professor Smith for the linguistic support. Finally I would like to extend my indebtedness to my family for their understanding, support, encouragement and sacrifice throughout my study.

References

Acott, T.S. and Kelley, M.J. (2008) Extracellular matrix in the trabecular meshwork. Exp Eye Res. 86, 543-561.

The AIGS Investigators. (2000) The Advanced Glaucoma Intervention Study (AGIS): 7. The relationship between control of intraocular pressure and visual field deterioration. Am J Ophthalmol. 130, 429-440.

Akaishi, T., Ishida, N., Shimazaki, A., Hara, H., and Kuwayama, Y. (2005) Continuous monitoring of circadian variations in intraocular pressure by telemetry system throughout a 12-week treatment with timolol maleate in rabbits. J Ocul Pharmacol Ther. 21, 436-444.

Ammar, D.A. and Kahook, M.Y. (2011) Effects of glaucoma medications and preservatives on cultured human trabecular meshwork and non-pigmented ciliary epithelial cell lines. Br J Ophthalmol. 95, 1466-1469.

Avizienyte, E., Fincham, V.J., Brunton, V.G., and Frame, M.C. (2004) Src SH3/2 domain-mediated peripheral accumulation of Src and phosphor-myosin is linked to deregulation of E-cadherin and the epithelial-mesenchymal transition. Mol Biol Cell. 15, 2794-2803.

Bradley, J.M., Vranka, J., Colvis, C.M., Conger, D.M., Alexander, J.P., Fisk, A.S., Samples, J.R., and Acott, T.S. (1998) Effect of matrix metalloproteinases activity on outflow in perfused human organ culture. Invest Ophthalmol Vis Sci. 39, 2649-2658.

Burke, A.G., Zhou, W., O'Brien, E.T., Roberts, B.C., and Stamer W.D. (2004) Effect of hydrostatic pressure gradients and Na_2EDTA on permeability of human Schlemm's canal cell monolayers. Curr Eye Res. 28, 391-398.

Camras, C.B., and Hedman, K. for the US Latanoprost Study Group. (2003) Rate of response to latanoprost or timolol in patients with ocular hypertension or glaucoma. J Glaucoma. 12, 466-469.

Choplin, N., Bernstein, P., Batoosingh, AL, and Whitcup, S.M.; for the Bimatoprost/Latanoprost Study Group. (2004) A randomized, investigator-masked comparison of diurnal responder rates with bimatoprost and latanoprost in the lowering of intraocular pressure. Surv Ophthalmol. 49, S19-S25.

Coleman, A.L. and Miglior, S. (2008) Risk factors for glaucoma onset and progression. Surv Ophthalmol. 53, S3-S10.

Collaborative Normal-Tension Glaucoma Study Group. (1998) Comparison of glaucomatous progression between untreated patients with normal-tension glaucoma and patients with therapeutically reduced intraocular pressures. Am J Ophthalmol. 126, 487-497.

Crosson, C.E., Sloan, C.F., and Yates, P.W. (2005) Modulation of conventional outflow facility by the adenosine A1 agonist N6-cyclohexyladenosine. Invest Ophthalmol Vis Sci. 46, 3795-3799.

Elliott, J., Zheleznova, N.N., and Wilson, P.D. (2011) c-Src inactivation reduces renal epithelial cell-matrix adhesion, proliferation, and cyst formation. Am J Physiol Cell Physiol. 301, C522-C529.

Fincham, V.J., Chudleigh, A., and Frame, M.C. (1999) Regulation of p190 Rho-GAP by v-Src is linked to cytoskeletal disruption during transformation. J Cell Sci. 112, 947-956.

Fuchshofer, R. and Tamm, E.R. (2009) Modulation of extracellular matrix turnover in the trabecular meshwork. Exp Eye Res. 88, 683-688.

Fukunaga, T., Ikesugi, K., Nishio, M., Sugimoto, M., Sasoh, M., Hidaka, H., and Uji, Y. (2009) The effect of the Rho-associated protein kinase inhibitor, HA-1077, in the rabbit ocular hypertension model induced by water loading. Curr Eye Res. 34, 42-47.

Gabelt, B.T. and Kaufman, P.L. (2003) Aqueous humor hydrodynamics. In Adler's Physiology of the Eye. Kaufman, P.L. and Alm, A., eds. 10th ed. (St. Louis, MO: Mosby), pp. 237-289.

Gabelt, B.T. and Kaufman, P.L. (2005) Changes in aqueous humor dynamics with age and glaucoma. Prog Retin Eye Res. 24, 612-637.

Goel, M., Picciani, R.G., Lee, R.K., and Bhattacharya, S.K. (2010) Aqueous humor dynamics: A review. The Open Ophthal J. 4, 52-59.

Hanke, J.H., Gardner, J.P., Dow, R.L., Changelian, P.S., Brissette, W.H., Weringer, E.J., Pollok, B.A., and Connelly, P.A. (1996) Discovery of a novel, potent, and Src family-selective tyrosine kinase inhibitor. J Biol Chem. 271, 695-701.

Harburger, D.S. and Calderwood, D.A. (2009) Integrin signalling at a glance. J Cell Sci. 122, 159-163.

Honjo, M., Tanihara, H., Inatani, M., Kido, N., Sawamura, T., Yue, B.Y.J.T., Narumiya, S., and Honda, Y. (2001) Effects of rho-associated protein kinase

inhibitor Y-27632 on intraocular pressure and outflow facility. Invest Ophthalmol Vis Sci. 42, 137-144.

Humphries, J.D., Byron, A., and Humphries, M.J. (2006) Integrin ligands at a glance. J Cell Sci. 119, 3901-3903.

Johnstone, M.A. (2009) Aqueous humor outflow system overview. In Becker-Shaffer's Diagnosis and Therapy of the Glaucomas. Stamper, R.L., Lieberman, M.F., and Drake, M.V., eds. (St. Louis: MO: Mosby), pp. 25-46.

Jones, R.J., Avizienyte, E., Wyke, A.W., Owens, D.W., Brunton, V.G., and Frame, M.C. (2002) Elevated c-Src is linked to altered cell-matrix adhesion rather than proliferation in KM12C human colorectal cancer cells. Br J Cancer. 87, 1128-1135.

Kaneko, E., Wada, T., Minagawa, Y., and Inoue, Y. (2012) Pharmacological profile and clinical efficacy of brimonidine tartrate (AIPHAGAN® ophthalmic solution 0.1%). Folia Pharmacol Jpn. 140, 177-182.

Kass, M.A., Gordon, M.O., Gao, F., Heuer, D.K., Higginbotham, E.J., Johnson, C.A., Keltner, J.L., Miller, J.P., Parrish, R.K, and Wilson, M.R. for the Ocular Hypertension Treatment Study Group. (2010) Delaying treatment of ocular hypertension: the ocular hypertension treatment study. Arch Ophthalmol. 128, 276-287.

Li, A.F., Tane, N., and Roy, S. (2004) Fibronectin overexpression inhibits trabecular meshwork cell monolayer permeability. Mol Vis. 10, 750-757.

Lu, Z., Overby, D.R., Scott, P.A., Freddo, T.F., and Gong, H. (2008) The mechanism of increasing outflow facility by rho-kinase inhibition with Y-27632 in bovine eyes. Exp Eye Res. 86, 271-281.

Okka, M., Tian, B., and Kaufman, P.L. (2004) Effects of latrunculin B on outflow facility, intraocular pressure, corneal thickness, and miotic and accommodative responses to pilocarpine in monkeys. Trans Am Ophthalmol Soc. 102, 251-257.

Peng, F., Zhang, B., Wu, D., Ingram, A.J., Gao, B., and Krepinsky, J.C. TGFβ-induced RhoA activation and fibronectin production in mesangial cells require caveolae. Am J Physiol Renal Physiol. 295, F153-F164.

Playford, M.P. and Schaller, M.D. (2004) The interplay between Src and integrins in normal and tumor biology. Oncogene. 23, 7928-7946.

Pollard, T.D. and Borisy, G.G. (2003) Cellular motility driven by assembly and disassembly of actin filaments. Cell. 112, 453-465.

Quigley, H.A. (1996) Number of people with glaucoma worldwide. Br J Ophthalmol. 80, 389-393.

Quigley, H.A. (2011) Glaucoma. Lancet. 377, 1367-1377.

Rao, P.V., Deng, P.F., Kumar, J., and Epstein, D.L. (2001) Modulation of aqueous humor outflow facility by the Rho kinase-specific inhibitor Y-27632. Invest Ophthalmol Vis Sci. 42, 1029-1037.

Russ, P.K., Kupperman, A.I., Presley, S.H., Haselton, F.R., and Chang, M.S. (2010) Inhibition of RhoA signaling with increased Bves in trabecular meshwork cells. Invest Ophthalmol Vis Sci. 51, 223-230.

Santas, A.J., Bahler, C., Peterson, J.A., Filla, M.S., Kaufman, P.L., Tamm, E.R., Johnson, D.H., and Peters, D.M. (2003) Effect of heparin Ⅱ domain of fibronectin on aqueous outflow in cultured anterior segments of human eyes. Invest Ophthalmol Vis Sci. 44, 4796-4804.

Thomas, S.M. and Brugge, J.S. (1997) Cellular functions regulated by Src family kinases. Annu Rev Cell Dev Biol. 13, 513-609.

Tian, B. and Kaufman, P.L. (2005) Effects of the Rho kinase inhibitor Y-27632 and the phosphatase inhibitor calyculin A on outflow facility in monkeys. Exp Eye Res. 80, 215-25.

Tokushige, H., Inatani, M., Nemoto, S., Sakaki, H., Katayama, K., Masayoshi Uehata, M., and Tanihara, H. (2007) Effects of topical administration of Y-39983, a selective rho-associated protein kinase inhibitor, on ocular tissues in rabbits and monkeys. Invest Ophthalmol Vis Sci. 48, 3216-3222.

Ueda, J., Wentz-Hunter, K., and Yue, B.Y. (2002) Distribution of myocilin and extracellular matrix components in the juxtacanalicular tissue of human eyes. Invest Ophthalmol Vis Sci. 43, 1068-1076.

Weinreb, R.N. (2007) Glaucoma neuroprotection: What is it? Why is it needed? Can J Ophthalmol. 42, 396-398.

Weinreb, R.N. and Khaw, P.T. (2004) Primary open-angle glaucoma. Lancet. 363, 1711-1720.

Williams, R.D., Novack, G.D., Haarlem, T.V., and Kopczynski, C. on behalf of AR-12286 phase 2A study group. (2011) Ocular hypotensive effect of the rho kinase inhibitor AR-12286 in patients with glaucoma and ocular hypertension. Am J Ophthalmol. 152, 834-841.

Zhang, M., Maddala, R., and Rao, P.V. (2008) Novel molecular insights into RhoA GTPase-induced resistance to aqueous humor outflow through the trabecular meshwork. Am J Physiol Cell Physiol. 295, C1057-C1070.

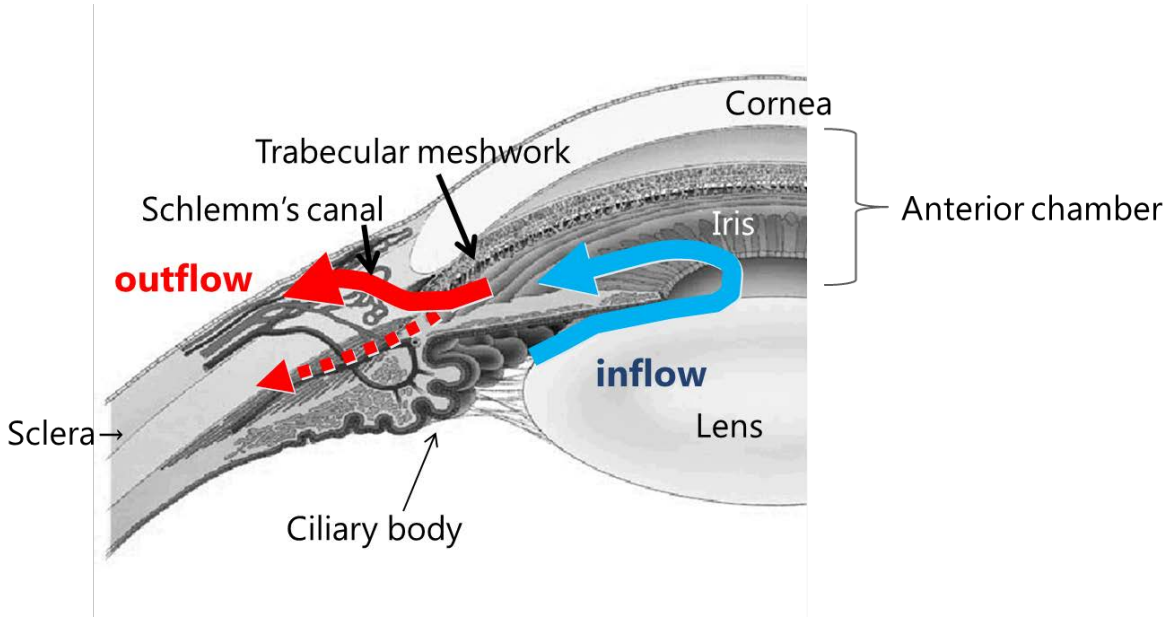

Figure 1. Structure of the anterior chamber angle and flow of aqueous humor in the eye

Aqueous humor is produced at non-pigmented epithelium of ciliary body, and flows in the anterior chamber through the space between lens and iris, and leaves the eye via outflow pathways at the anterior chamber angle. Outflow pathway consists of the conventional (red solid line) and the uveoscleral (red dash line) outflow routes. Main tissues composing the conventional outflow route are the trabecular meshwork and the Schlemm's canal.

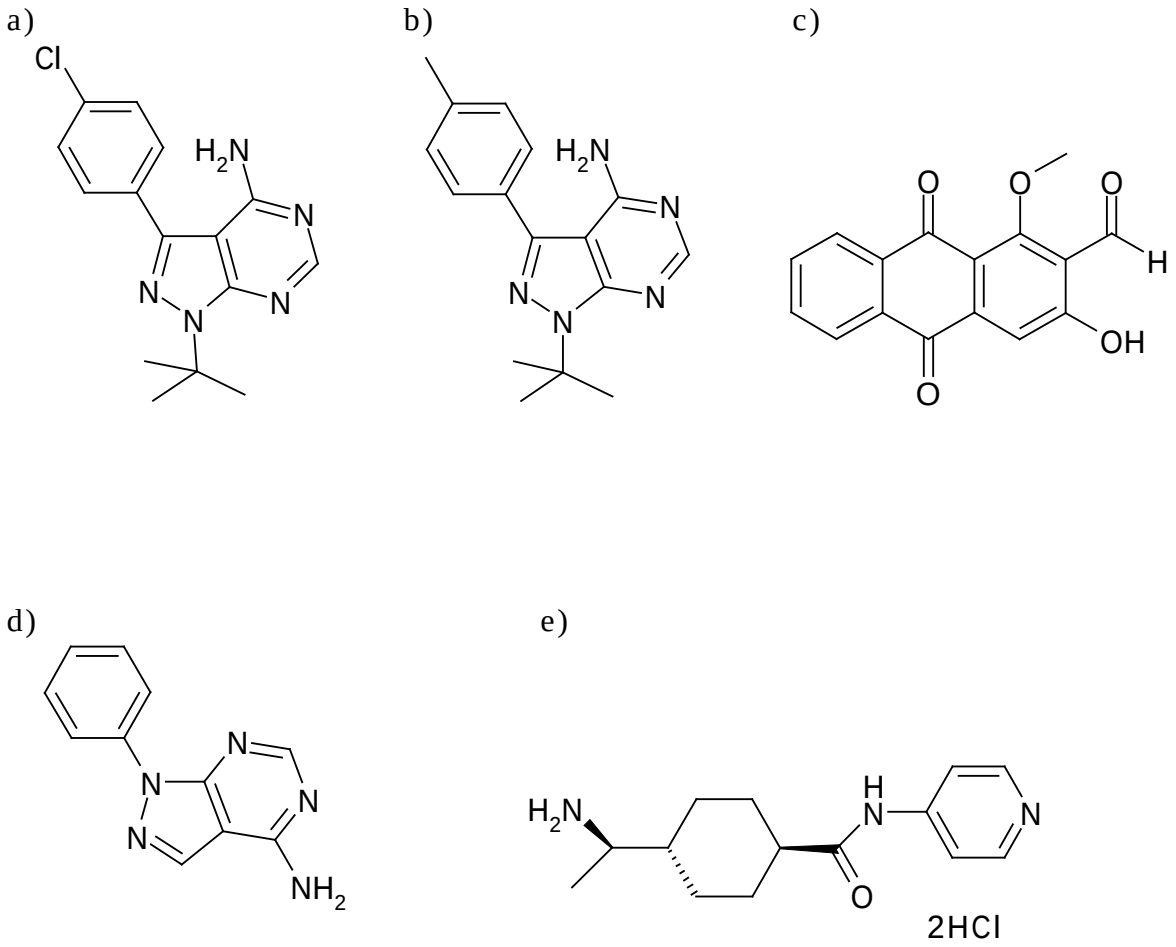

Figure 2. Chemical structures of the evaluated compounds

PP2 (a), PP1(b), damnacanthal (c) are SFK inhibitors. PP3 (d) is a negative conotrol of PP2 (no kinase inhibitory activity to src-family tyrosine kinases). Y-27632 dihydrochloride (e) is a Rock inhibitor.

a)

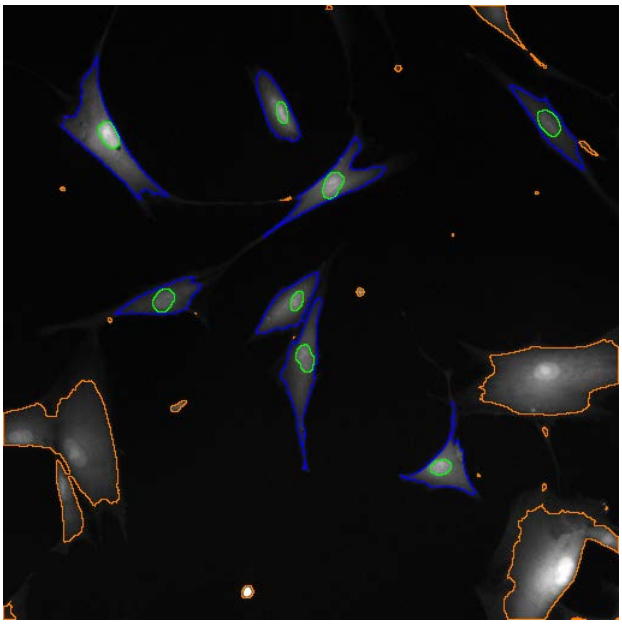

b)

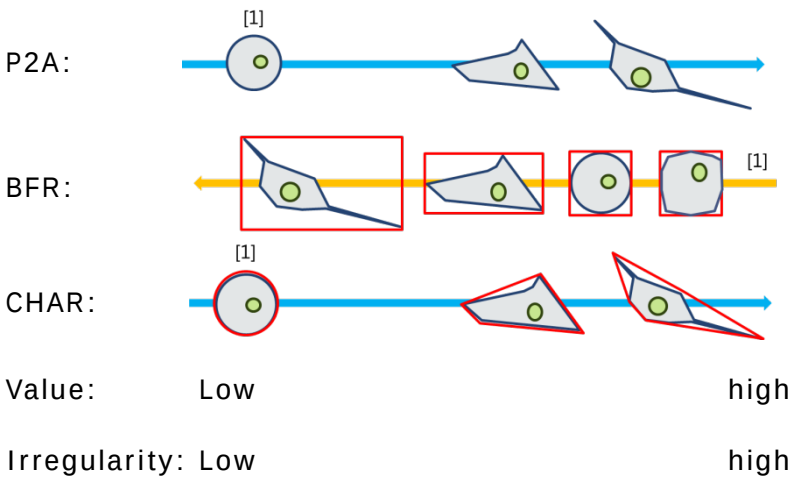

Figure 3. An example of analysis by ArrayScan and images of relationship among morphology, irregularity, and index values

a) An example of analysis by ArrayScan. The size of the captured field by the 20x objective lens is 512x512 pixels (0.645 μm/pixel). Colors represent: green, nuclei; blue, selected cell for analysis; orange, rejected cell due to the attachment to the edge of the field. Objects having more than one nucleus were also rejected.

b) Images of relationship morphology, irregularity, index values in P2A, BFR, and CHAR. Red line represents a bounding rectangle box in BFR or a convex hull area in CHAR. A value deviated more from 1 unit indicates acquiring irregular shape: a value higher than 1 unit in P2A and CHAR; a value lower than 1 unit in BFR.

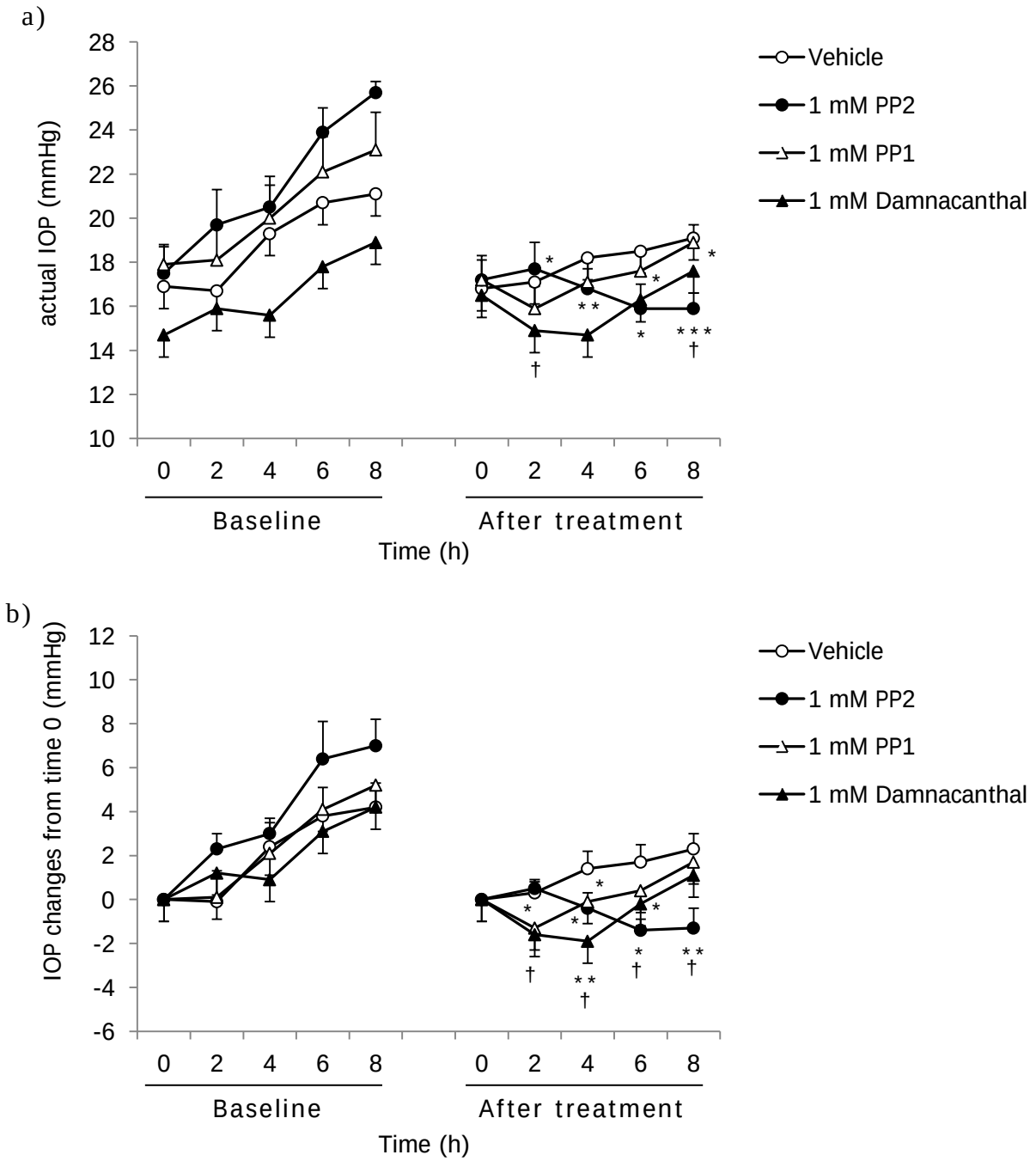

Figure 4. Changes in IOP after administraton of SFK inhibitors.

PP2, PP1 or damnacanthal at 1 mM, or vehicle, was intracamerally injected into one eye in ocular normotensive rabbits on the treatment day. IOP change after drug administration was compared to each scheduled time point of baseline. Baseline was measured 2 days before the treatment day without drug administration. Data represent mean ± SE for 5 animals. * $p < 0.05$, ** $p < 0.01$, *** $p < 0.001$ relative to baseline (paired *t*-test). † $p < 0.05$ relative to the vhicle-treated group (Student's *t*-test).

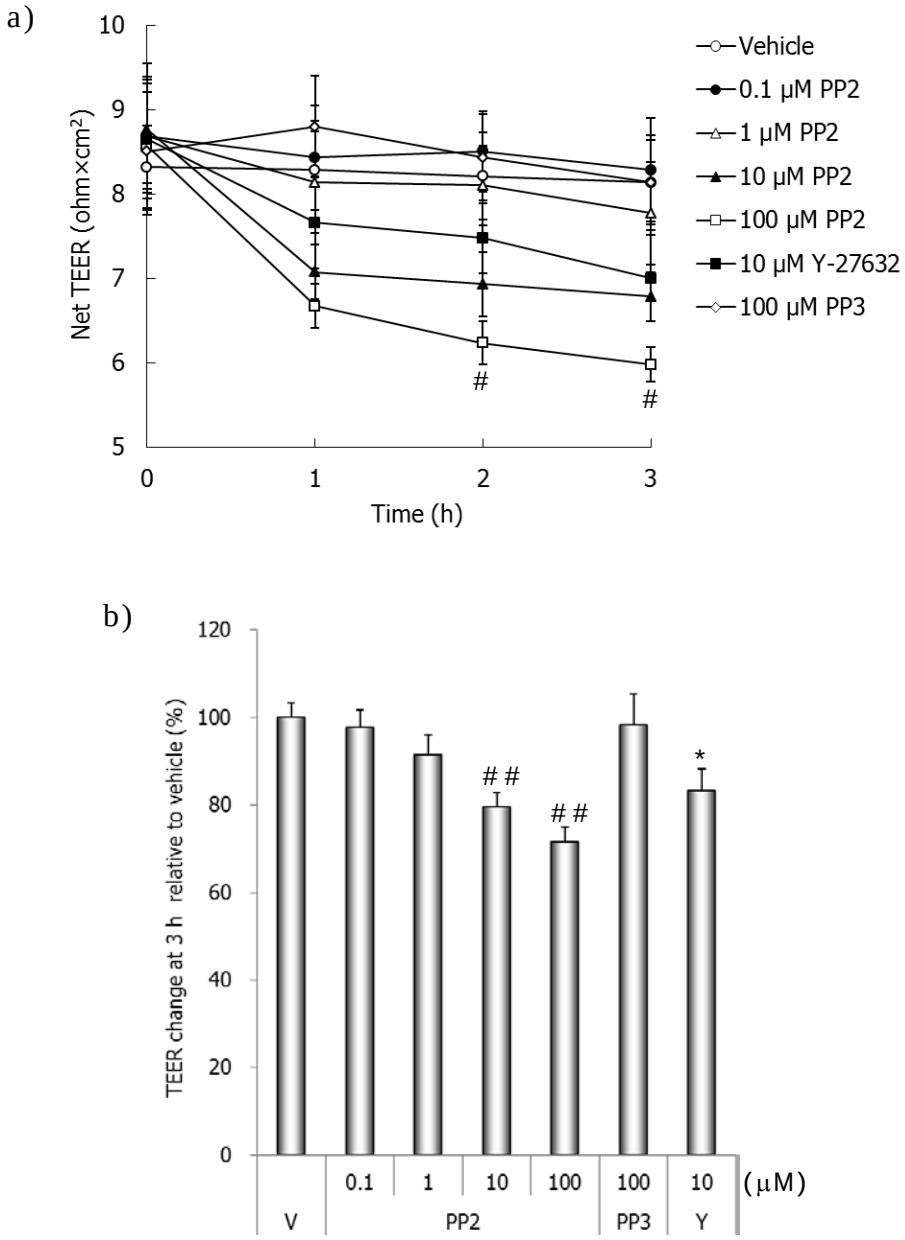

Figure 5. Effect of PP2 on TEER across TM cell layers.

TM cells, in the upper chamber of membrane inserts, were treated for 3 h with vehicle (V), PP2 at 0.1, 1, 10, or 100 μM, PP3 at 100 μM, or Y-27632 (Y) at 10 μM. Net TEER was calculated by subtracting a blank value from measured values in each well with cells. Data represent mean ± SE for 3 independent experiments. Each experiment was performed in triplicate. # $p < 0.05$, ## $p < 0.01$ relative to vehicle by Dunnett multiple comparison test. * $p < 0.05$ relative to vehicle by Student's *t*-test.

a) Time-dependent changes in net TEER.

b) Changes in TEER at 3 h from the pretreatment value for each group relative to the vehicle-treated group.

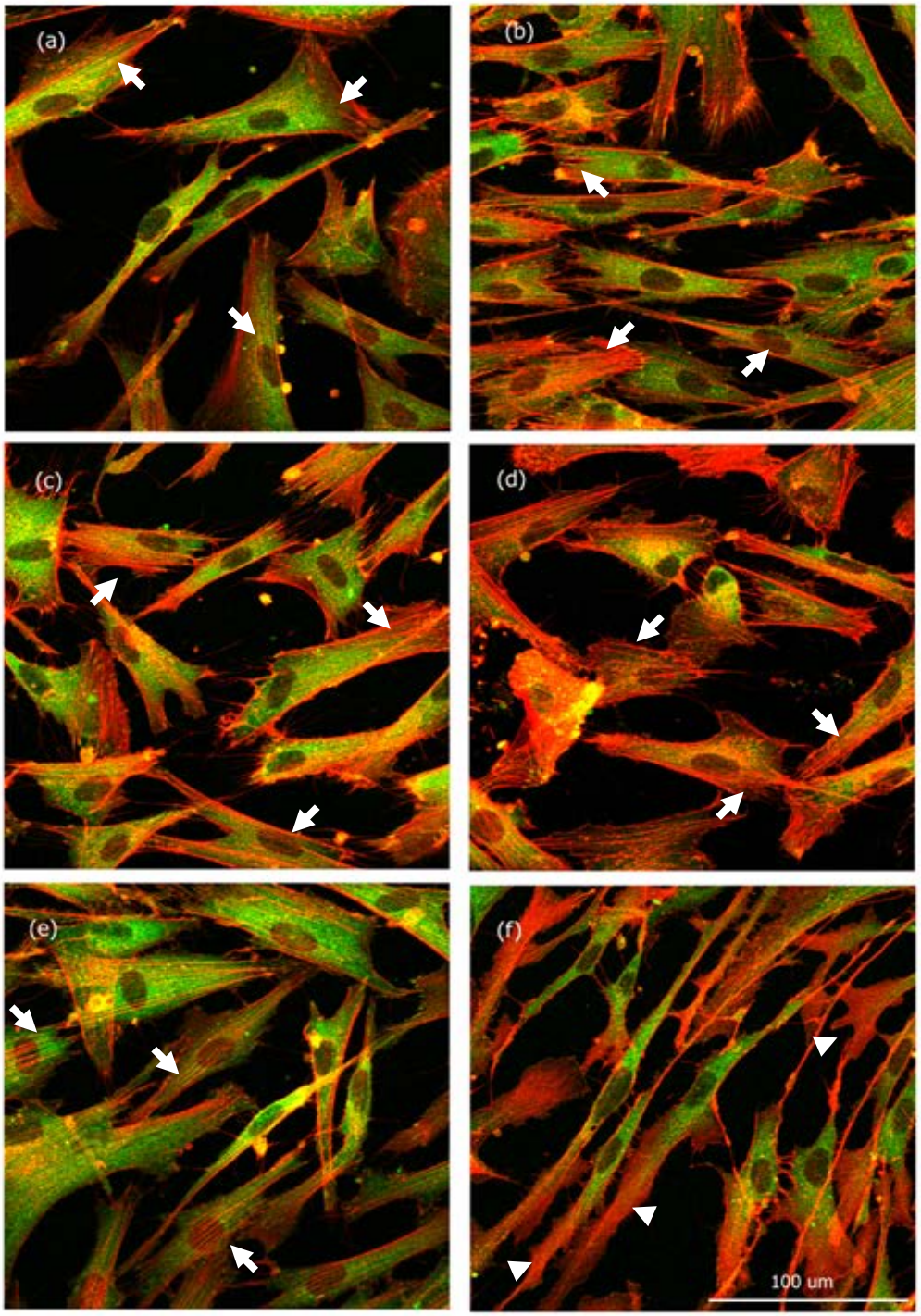

Figure 6. Changes in TM cell morphology.

TM cells were treated for 3 h with vehicle, PP2 at 0.1, 1, 10, or 100 μM, or Y-27632 at 10 μM. After the drug treatment, vinculin (green) and F-actin (red) were stained. Arrows indicate representative actin stress fibers and arrowheads indicate diffuse staining of actin (disappearance of stress fiber).

a) Vehicle, b) 0.1 μM PP2, c) 1 μM PP2, d) 10 μM PP2, e) 100 μM PP2, f) 10 μM Y-27632.

Table 1. The average of analyzed cell number on ArrayScan

	Vehicle	PP2				Y-27632 (10 μM)
		0.1 μM	1 μM	10 μM	100 μM	
The average of analyzed cell number	688.0 ± 216.4	704.7 ± 219.9	597.7 ± 190.8	376.0 ± 74.4	367.7 ± 88.5	774.0 ± 174.1

TM cells were treated for 3 h with vehicle, PP2 at 0.1, 1, 10, or 100 μM or Y-27632 at 10 μM. One hour before the end of drug treatment, cells were stained with calcein, and did with hoechst33343 after fixation. The number of cells is a total amount of 8 well consisting of 10 visual fields. The data represent mean ± SD for 3 independent experiments.

Table 2-a. Actual values of morphological indexes

Index	Vehicle	PP2				Y-27632 (10 μM)
		0.1 μM	1 μM	10 μM	100 μM	
Area (pixels)	1004.5 ± 57.6	1069.1 ± 130.1	1052.1 ± 142.8	1099.5 ± 110.9	1143.6 ± 147.7	1155.8 ± 136.2
P2A (units)	2.28 ± 0.11	2.35 ± 0.11	2.31 ± 0.12	2.15 ± 0.16	2.33 ± 0.06	2.75 ± 0.09**
BFR (units)	0.60 ± 0.01	0.60 ± 0.01	0.61 ± 0.01	0.62 ± 0.02	0.61 ± 0.01	0.53 ± 0.01***
CHAR (units)	1.16 ± 0.00	1.17 ± 0.01	1.14 ± 0.01	1.12 ± 0.02##	1.14 ± 0.01	1.31 ± 0.01***

Table 2-b. Changes in morphological indexes relative to vehicle (%)

Index	Vehicle	PP2				Y-27632 (10 μM)
		0.1 μM	1 μM	10 μM	100 μM	
Area	100	106.2 ± 6.7	104.4 ± 8.3	109.3 ± 5.0	113.6 ± 9.9	115.1 ± 13.0
P2A	100	103.2 ± 0.1	101.4 ± 0.6	94.6 ± 3.2	102.3 ± 2.8	120.9 ± 8.1*
BFR	100	98.9 ± 1.6	100.8 ± 0.7	103.4 ± 2.0#	101.3 ± 0.7	87.6 ± 0.2***
CHAR	100	100.9 ± 0.7	98.9 ± 0.5	96.7 ± 1.2###	98.3 ± 0.3#	113.1 ± 1.2**

TM cells were treated for 3 h with vehicle, PP2 at 0.1, 1, 10, or 100 μM or Y-27632 at 10 μM. Data represent mean ± SD for 3 independent experiments. Data for each experiment consisted of 8 wells. Table 2-a shows the actual values for each index, while changes in each index relative to the vehicle-treated group (100%) are shown in Table 2-b. # $p < 0.05$, ## $p < 0.01$, ### $p < 0.001$ relative to vehicle by Dunnett multiple comparison test. * $p < 0.05$, ** $p < 0.01$, *** $p < 0.001$ relative to vehicle by Aspin-Welch's *t*-test.

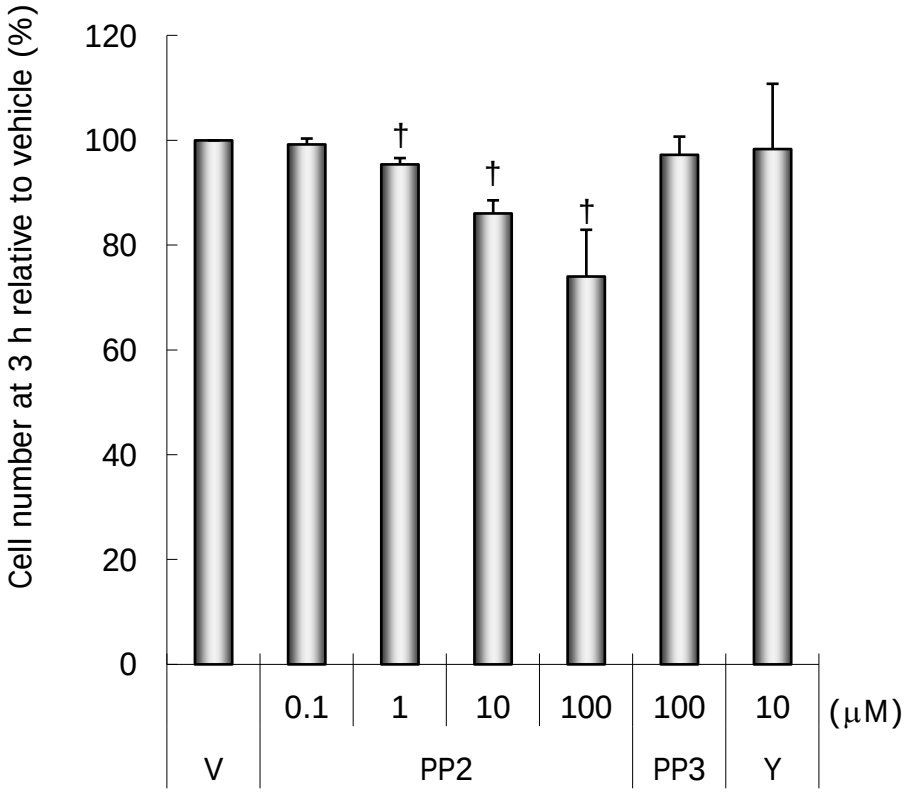

Figure 7. Effect of PP2 on TM cell adhesion to tissue culture-treated surface.

TM cells were treated for 3 h with vehicle (V), PP2 at 0.1, 1, 10, or 100 μM, PP3 at 100 μM, or Y-27632 (Y) at 10 μM. One hour before the end of drug treatment, cells were stained with calcein. After the drug treatment, cells were washed and fixed, and absorbance at excitation 485 nm/emission 535 nm was measured. The number of attached cells is expressed as a ratio to the number in the vehicle-treated group. Data represent mean ± SD for 4 independent experiments. Each experiment was performed in octuplicate. † $p < 0.05$ relative to vehicle by Steel multiple comparison test.

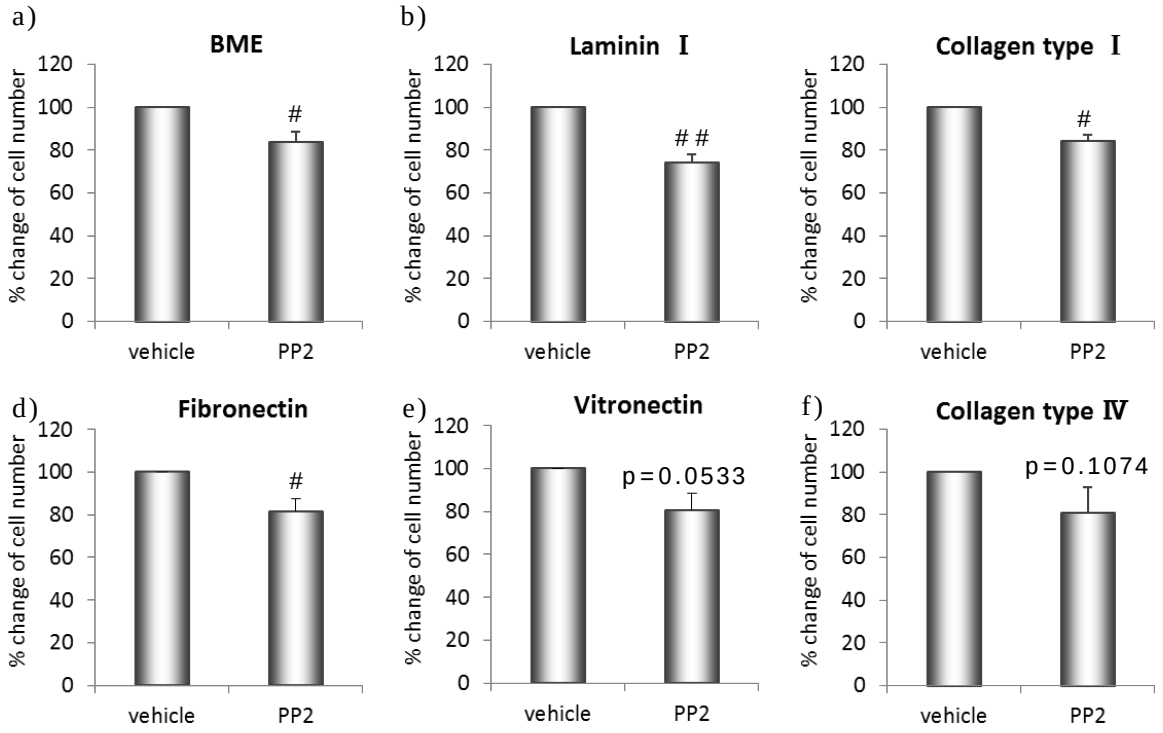

Figure 8. Effect of PP2 on TM cell adhesion to ECM protein-coated surfaces.

TM cells were treated for 3 h with vehicle or 100 μM PP2. One hour before the end of drug treatment, cells were stained with calcein. After treatment, cells were fixedd and washed, and absorbance at excitation 485 nm/emission 535 nm was then measured. The number of attached cells is expressed as a ratio to the number in the vehicle-treated group for each coating condition. Data represent mean ± SD for 3 independent experiments. Each experiment was performed in in quadruplicate or sextuplicate. # $p < 0.05$, ## $p < 0.01$ relative to vehicle by Aspin-Welch's *t*-test. p values shown in e) and f) are the results of Aspin-Welch's *t*-test.

Surfaces were coated with a) BME, b) laminin I, c) collagen type I, d) fibronectin, e) vitronectin, and f) collagen type IV.

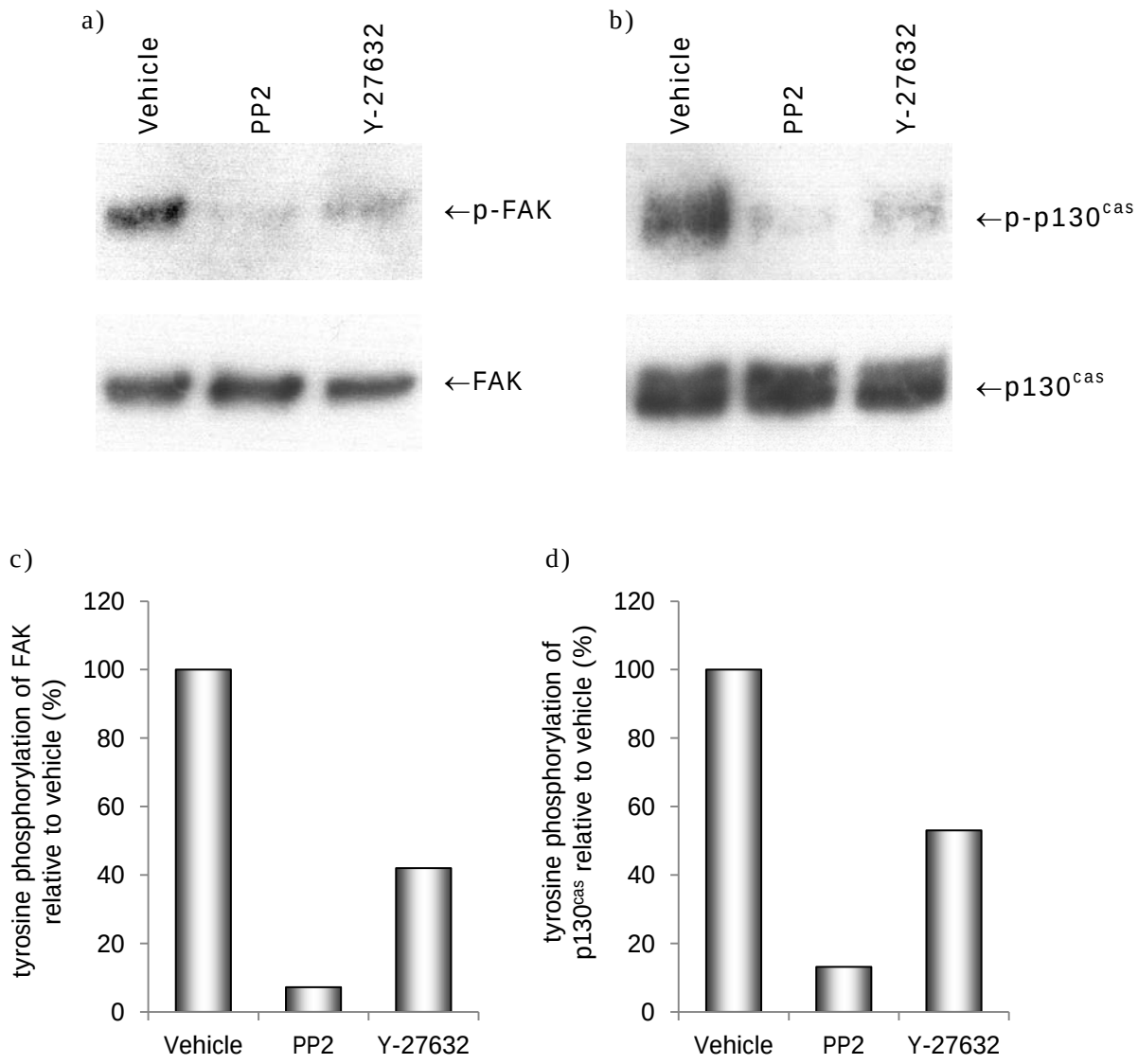

Figure 9. Changes in tyrosine phosphorylation of FAK and p130^{cas} in TM cells

TM cells were treated for 3 h with vehicle, 100 μM PP2, or 10 μM Y-27632. Extracted proteins were analyzed by western blot, first using anti-phospho-FAK or anti-phospho-p130^{cas} antibody (upper panels: a, FAK [125 kDa]; b, p130^{cas} [130 kDa]) and then using total antibodies to each protein (lower panels of a and b). Quantitative analysis of the amount of tyrosine phosphorylation relative to total proteins was performed using the image analyzer: c, FAK; d, p130^{cas}. Data represent mean for 2 independent experiments. Each sample was measured in duplicate.

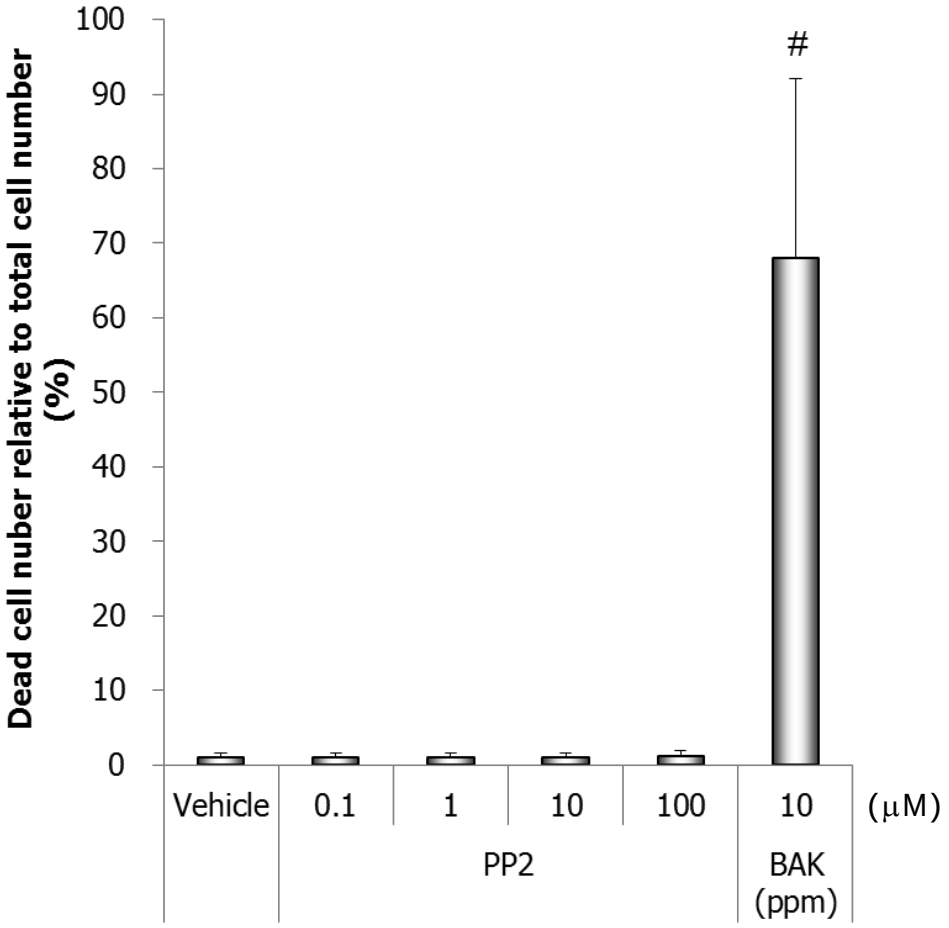

Figure 10. PP2 does not cause cell death of TM cells

TM cells were treated for 3 h with vehicle, PP2 at 0.1, 1, 10, or 100 μM, or BAK at 10 ppm. After the drug treatment, assay reagent including AAF-Glo substrate was added, and luminescence was measured to determine the number of dead cells. Subsequently, lysis reagent including digitonin was added, and luminescence was again measured to determine the number of total cells. Cell death is expressed as a ratio of the number of dead cells to the number of total cells. Data represent mean ± SD for 3 independent experiments. Each experiment was performed in octuplicate. # $p < 0.05$ relative to vehicle by Aspin-Welch's *t*-test.